Experimental investigation on performance improvement of thermoelectric generator based on phase change materials and heat transfer enhancement

Yijiang Wang [a, b]*, Yizhu Peng [a], Kehui Guo [a], Xiaofeng Zheng [b], Jo Darkwa [b], Hua Zhong [c]

[a] State key laboratory for Geomechanics and Deep Underground Engineering, School of Mechanics and Civil Engineering, China University of Mining and Technology, Xuzhou 221116, China

[b] Faculty of Engineering, University of Nottingham, University Park, Nottingham NG7 2RD, UK

[c] School of Architecture, Design and the Built Environment, Nottingham Trent University, Nottingham NG1 4BU, UK

* Corresponding author: yjwang@cumt.edu.cn (Y. Wang).

Abstract: Thermoelectric application has been widely researched due to its various advantages. Its use has been limited to niche industrial applications and exploratory research development due to the poor economic viability. It is essential to achieve the optimum system performance to improve the economic viability. In view of that, this study aims to improve the system performance by adopting the phase change materials (PCM) and heat transfer enhancement to establish improved thermal conditions. It experimentally investigates the effects of PCM and heat transfer enhancement on the open-circuit voltage and electrical energy of thermoelectric generator (TEG) system. Results indicate that the phase change temperature, thickness and thermal conductivity of PCM have a considerable impact on the electrical energy generated by TEG. An increase in absorption coefficient by surface coating can lead to an increase in electrical energy. However, the total electrical energy under forced convection is not obviously increased comparing with the natural convection case. The results achieved in this study indicate that suitable PCM and heat transfer enhancement measures should be considered according to the working conditions of TEG.

Keywords: solar thermoelectric generator; phase change materials; heat transfer enhancement; absorption coefficient; heat convection; electrical energy

1. Introduction

The intensive use of fossil fuels including coal-fired power plants is responsible for various environmental issues such as greenhouse emission, global warming and air pollution [1, 2]. Recently, electric power generation from renewable resources such as solar energy, biomass energy and wind energy has received considerable attention as the renewable resources can provide sustainable and green electricity with reduced carbon dioxide emissions [3-6]. For instance, thermoelectric power generation technology based on Seebeck effect can realize the direct conversion of thermal energy to electrical energy by using thermoelectric generators (TEG), which were often used for the recovery and utilization of low-grade heat sources such as geothermal energy, solar energy and industrial waste heat [7].

Typically, a TEG consists of arrays of N-P semiconductor chips which are electrically connected in series and thermally connected in parallel, and usually covered by ceramic substrates [8]. The key thermoelectric properties of a TEG include the Seebeck coefficient, the electrical conductivity and thermal conductivity of the thermoelectric material, which are usually characterized by a dimensionless value: figure-of-merit (ZT) [9, 10]. Despite its low ZT, the thermoelectric generation technology has been utilized in a wide range of areas such as aerospace facilities, transport tools and industry utilities, in which a considerable amount of waste heat offers a great opportunity for making direct use, such as stoves [11, 12], vehicle waste heat [13], subsurface coal fires [14], solar energy [15-20] and industrial waste heat [21, 22].

Because the conversion efficiency is the key barrier to wide thermoelectric applications, ongoing efforts have been made by many researchers and scientists in material research to fundamentally improve the thermoelectric properties, thereby enhancing its commercial adoptability [23-26]. In the meantime, an increasing number of researches have also been ongoing at the system level to improve

its overall performance and economic viability [27-29]. Various approaches have been taken to achieve that goal and they mainly include innovative system design, novel heat harvesting concept and effective cooling design, etc. Table 1 summarizes the technical measures that have been undertaken to improve the overall system performance.

Table 1 Technical measures on enhanced performance of TEG.

Approach	Key findings
Heat dissipation	The heat transfer of cold side of TEG was enhanced by using liquid cooling in combination of novel heat exchanger design [30, 31]. Heat sink had a great effect on the performance of thermoelectric module as the heat dissipation could be improved [32].
Heat sourcing	Unconverted heat of domestic boiler was utilized through a thermal cycle, with the energy utilization efficiency up to 80% [33, 34]. The use of graphite sheets devices attributed to a great increase in the amount of solar energy absorbed [35, 36]. The spectrally-selective solar absorbers promoted the thermoelectric efficiency to 4.6% which was 7-8 times higher than that of the traditional solar TEG [37].
System design	TEG and exhaust pipe were connected by using heat pipes, with a maximum TEG thermal efficiency of 2.46% [38].

Among the various measures for improving thermoelectric system efficiency summarized in Table 1, the PCM-based approach has been favored by many researchers in the field as an effective method for establishing a stable and useful thermal condition for a prolonged operation. This can be achieved because PCM can store and release a large amount of thermal energy with a stable temperature through a solid-liquid phase change, which comes with a large amount of latent heat. In addition,

PCM also offer the flexibility of utilizing the latent heat at a time when an optimum thermal condition can be achieved to deliver an enhanced system energy output [39]. For instance, the latent heat stored in PCM can also be released at night to allow the thermoelectric system to have a continued generation of electrical energy [40, 41]. A few typical research studies are introduced herein to provide an insight into how PCM can be used to enhance the system performance of thermoelectric applications. Jaworski et al. [42] experimentally investigated the performance of TEG module coupled with PCM which indicated that PCM can be effectively used as both heat sink and heat source. Zhu et al. [43] designed an aircraft-specific TEG module coupled with a PCM storage and studied the power output characteristics. Results showed that PCM with a suitable melting temperature was critical to temperature control, which affected the power output. A two-stage thermoelectric generator was proposed to improve the performance of TEG system [44] in which the PCM heat sink of the first stage was utilized as the heat source of the second stage TEG. Experimental results indicated that the two-stage TEG system could generate 27% more electricity than the one-stage TEG system. PCM was employed on both sides of the TEG as the thermal management of TEG systems, which showed that PCM could considerably enhance duration of electricity generation under specific thermal boundary conditions compared to systems without PCM box [45]. In addition, an innovative method was explored to achieve the light manipulation through optical and thermal management, which represented a promising approach to achieve a desired operating temperature for an improved TEG performance through a combination of reduced optical absorption and radiative cooling [46].

This paper presents an experimental investigation on the performance of a PCM-based TEG system under periodic radiation conditions, which is a further advancement of the traditional solar TEG system. In this study, an aluminum box containing PCM is used as the heat sink of the TEG system at the radiation stage and heat source at the subsequent cooling stage. The effect of phase change

temperature, thermal conductivity and thickness of PCM layer on the thermoelectric performance of the TEG system was experimentally investigated through the analysis of the open-circuit voltage and generated electrical energy. In addition, the influence of heat transfer enhancement measures including the improvement of absorption and convection coefficients on the system performance was also presented.

2. Test setup and arrangement

2.1. Experimental system

As shown in Fig. 1, the system consists of the thermoelectric generator, phase change materials (PCM) and aluminum container, radiation source and data collecting system.

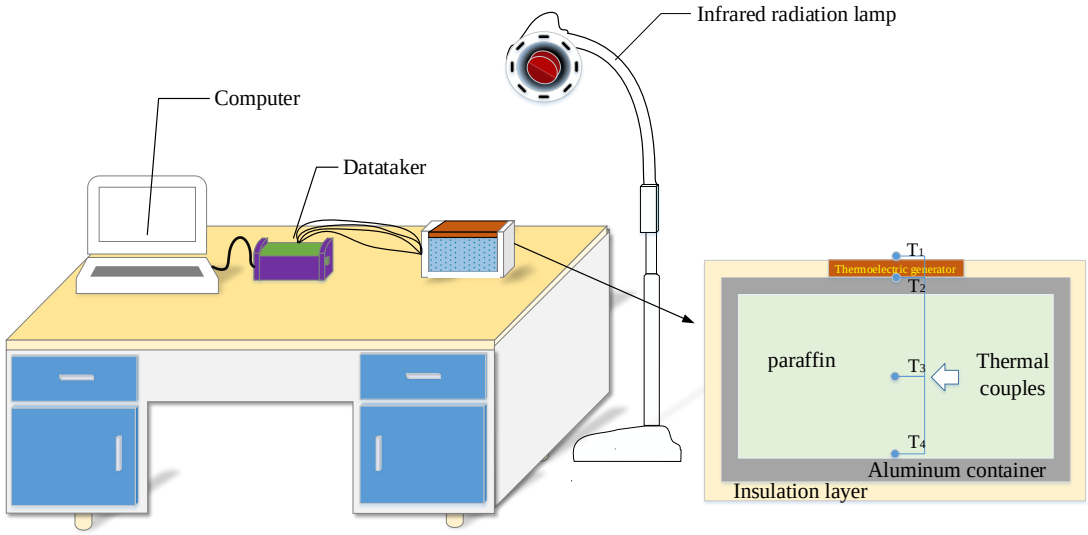

Fig. 1. Schematic of PCM-TEG system.

(1) Thermoelectric generator: The TEG1-241with thermoelectric material of Bi_2Te_3 was used in this study. The Seebeck coefficient and internal resistance of TEG1-241 at the room temperature are 0.103 V/°C and 6.95 Ω, respectively.

(2) Phase change materials: Paraffin (No.: 32#, 38# and 42#) was used as PCM owing to the excellent thermophysical properties listed in Table 2. The phase change temperature and enthalpy of PCM were tested by using Differential Scanning Calorimetry (DSC), as shown in Fig. 2. To reduce

the influence of material processing, two heating cycles and one cooling cycle were conducted in the DSC test. The melting phenomenon was observed when the temperature of paraffin was lower than its phase-transition temperature. The heat flow continued to sharply increase, in the meantime, the temperature of paraffin slowly increased. After the heat flow reached the maximum level, it then began to decrease gradually. The temperature corresponding to the maximum heat flow was generally believed to be the phase-transition temperature. It can be seen from Fig. 2 that the phase-change temperature was in the range of 31.14 ºC to 42.07 ºC for paraffin of 32#, 38# and 42#. The phase-change enthalpy of paraffin was computed by the integration of the heating energy during the phase-transition period, which was also presented in Fig. 2.

The PCM was stored in a container that was made of aluminum with a thermal conductivity of 218 W/(m·K). In order to reduce the heat loss of PCM through the container to the surrounding environment, all sides of the container except the top cover were insulated by an insulation layer made of polyurethane, as shown in Fig. 1. The thermal conductivity and specific heat capacity were measured by Hot Disk, with the range between 0.2984-0.2727 W/(m·K) and 1.2437-1.4647 kJ/(kg·K) respectively for paraffin of 32#, 38# and 42#. The density was tested by measuring cup and electronic balance.

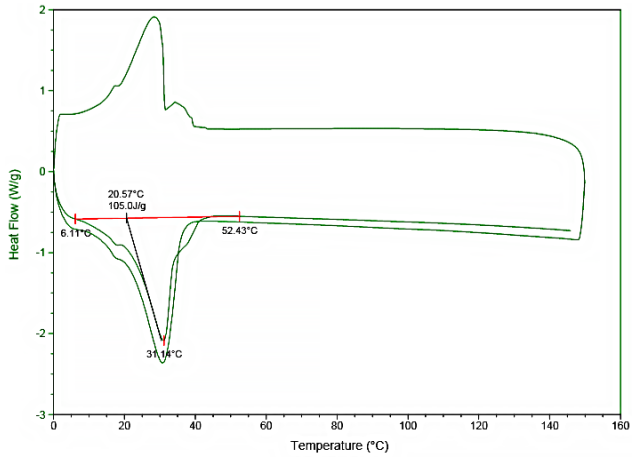

(a) 32#

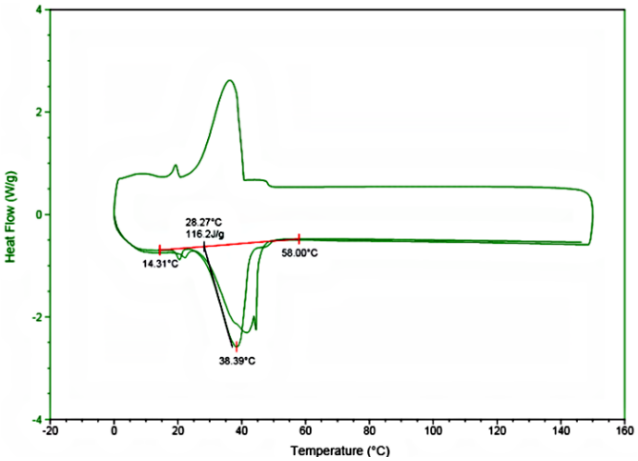

(b) 38#

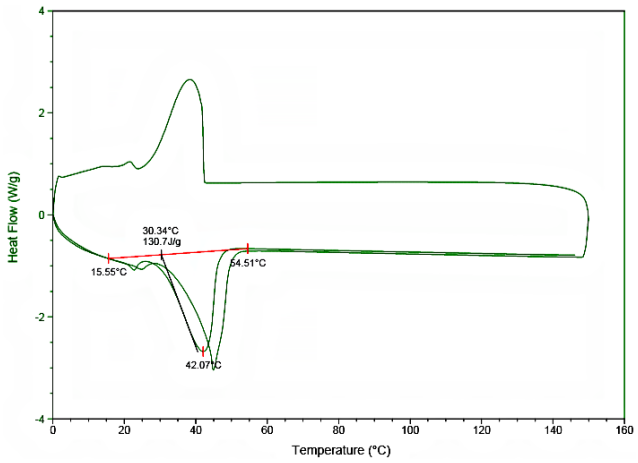

(c) 42#

Fig. 2. DSC testing results of PCM.

Table 2 Thermo-physical properties of PCM.

No.	Phase-change temperature (°C)	Enthalpy (kJ/kg)	Thermal conductivity (W/(m·K))	Specific heat capacity (kJ/(kg·K))	Density (kg/m³)
32#	31.14	105	0.2984	1.2516	810
38#	38.39	116.2	0.2838	1.4647	850
42#	42.07	130.7	0.2727	1.2437	900

(3) Radiation source: An infrared radiation light with ten radiative intensities was used in this study to simulate various levels of solar radiation. The radiation intensity was measured by a radiation tester with a distance of 0.3 m to the infrared lamp, ranging from 240 W/m^2 to 1330 W/m^2. The radiation distribution is relatively uniform when it is 0.3 m away from the light source.

2.2. Experiment scenarios

Three kinds of PCM with phase-transition temperature of 31.14 °C, 38.39 °C and 42.07 °C were used in this study, and the thickness of PCM layer was ranged from 0.01 m to 0.03 m. The graphite with the mass ratio in the range of 1%-4% was added into PCM to improve the thermal conductivity of PCM. The impact of PCM with different phase-change temperature, thickness of PCM, mass ratio

of graphite, surface treatment and forced convection coefficient at the TEG surface on the system performance was experimentally investigated. The detailed experiment scenarios are presented in Table 3. According to previous literatures [40, 43], the cycle time was set to 2 hours including 1 hour of radiation stage and 1 hour of cooling stage, and two cycles were conducted for all the experiments.

Table 3 Experiment scenarios.

Test No.	PCM	Thickness of PCM (m)	Mass ratio of graphite (%)	Surface treatment	Wind speed (m/s)
1	32#, 38#, 42#	0.03	0	Original	0
2	38#	0.03, 0.02, 0.01	0	Original	0
3	38#	0.03	0, 1, 2, 3, 4	Original	0
4	38#	0.03	1	Original, Coated	0
5	38#	0.03	1	Coated	0, 0 (radiation)-3 (cooling)

2.3. Measurement uncertainty

T-type thermocouple with an accuracy of ±0.5 ºC was used to measure the temperature of TEG and PCM. Data-taker and digital multimeter with accuracies of $\pm 0.13\times10^{-3}$ V and ±0.8% were used to measure voltage and current respectively. To ensure the accuracy of the experimental results, the sensor accuracy and measurement uncertainty were analyzed and listed in Table 4. The uncertainties were computed through the sensor accuracy and the Bessel equation of standard deviation. The equations of uncertainty for directed variables are presented by Eq. (1) [47]:

Table 4 Measurement accuracy and uncertainty.

Variables	Temperature	Voltage	Current
Sensor accuracy	±0.5 ºC	±0.13×10^{-3} V	±0.8%
Measurement uncertainty	±5%	±2%	±3%

$$u_{\mathrm{v}} = \sqrt{\Delta_{\mathrm{v}}^2 + \sigma_{\mathrm{v}}^2} \tag{1}$$

where u_{v} is the uncertainty of directed variables, Δ_{v} is the sensor accuracy of the variables, σ_{v} is the Bessel equation of standard deviation and the equation is described by Eq. (2):

$$\sigma_{\mathrm{v}} = \sqrt{\frac{\sum_{i}^{N}(x_i - \bar{x})^2}{N-1}} \tag{2}$$

where x_i and $\bar{x}$ are individual measured values and the mean value of individual measured values, N is the number of testing items. The measurement uncertainties of temperature, voltage and current are ±5%, ±2% and ±3% based on the calculated data respectively, which can be considered acceptable for the experimental set.

The power output of an applied thermoelectric application depends on the load resistance of the circuit. To achieve the maximum power output of TEG, the load resistance should be equal to the internal resistance of TEG [45]. Therefore, the maximum power output could be computed by multiplying the half of the open-circuit voltage and the half of the short-circuit current, as described by Eq. (3):

$$P_{\max} = \frac{1}{2}U_{\mathrm{oc}} \times \frac{1}{2}I_{\mathrm{sc}} \tag{3}$$

where $P_{\max}$ is the maximum power output, W; U_{oc} is the open-circuit voltage, V; I_{sc} is the short-circuit current, A. The short-circuit current can be calculated by Eq. (4):

$$I_{\mathrm{sc}} = U_{\mathrm{oc}} / R_{\mathrm{TEG}} \tag{4}$$

where R_{TEG} is the internal resistance of TEG. Therefore, the total electrical energy generated by TEG

can be computed by Eq. (5):

$$E = \int_0^t P_{\max} dt \tag{5}$$

where E is electrical energy, J; t is time, s.

3. Results and discussion

3.1 Effect of PCM

3.1.1. Phase-change temperature

Fig. 3 illustrates the variation of the open-circuit voltage and temperature of TEG and PCM (38#) under a thermal radiation intensity of 615 W/m^2. The temperature of TEG and PCM firstly increases at the radiation stage and then slowly decreases at the natural cooling stage. The temperature increase rate is larger than the temperature decrease rate owing to the greater heat exchange with the radiation source. In addition, the temperature of TEG and PCM at the second radiation and natural cooling stage is higher than that at the first stage. This may be attributed to the higher initial temperature of TEG and PCM at the beginning of the second cycle.

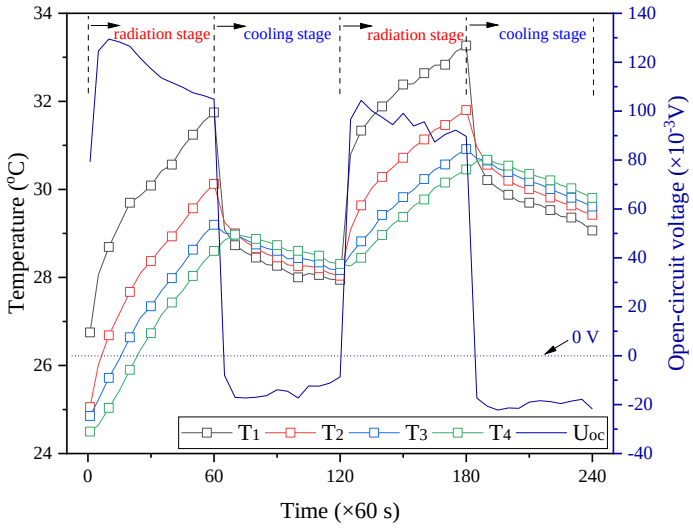

Fig. 3. Open-circuit voltage and temperature of TEG.

In addition, the open-circuit voltage significantly increases in a very short time and then slowly decreases at the radiation stage. When the radiation lamp is shut down, the open-circuit voltage

gradually turns into negative value from the positive output, which indicates that the TEG module coupled with the PCM continues to generate electrical energy even if there is no active input of thermal radiation. The reason is that the thermal energy stored in the PCM with large phase change latent heat can also be transferred to the TEG at the natural-cooling stage, which results in a temperature difference between two surfaces of the TEG. However, the open-circuit voltage at the cooling stage is lower than that at the radiation stage owing to the reduced temperature difference. The open-circuit voltage at the radiation and natural-cooling stage in the second cycle is respectively lower and higher than that in the first cycle due to different levels of initial temperatures of the TEG and PCM.

The PCM temperature (T_3) and open-circuit voltage of different kinds of PCM under a radiation intensity of 615W/m^2 are illustrated in Fig. 4, which shows the temperature of PCM increases at the radiation stage and decreases slowly at the cooling stage, and temperature range also varies with different kinds of PCM owing to the different heat transfer rates at the radiation and cooling stage. For instance, the maximum temperature of 28.0 ºC, 29.2 ºC and 29.6 ºC is achieved for the PCM of 32#, 38# and 42# respectively at the first radiation stage. In addition, the temperature of the 32# PCM drastically increases at the second radiation stage. It is highly likely attributed to the fact that the phase change process occurs when the temperature is lower than the phase transition temperature. The open-circuit voltage of different types of PCM is demonstrated in Fig. 4 (b), which shows that the open-circuit voltage of the 32# PCM is higher than that of other two PCM at the radiation stage. The lower the PCM temperature, the larger the temperature difference between two surfaces of TEG at the radiation stage is. Therefore, a higher open-circuit voltage can be obtained from a lower PCM temperature. However, a lower PCM temperature at the cooling stage results in a decreased open-circuit voltage owing to a decreased temperature difference between two surfaces of the TEG.

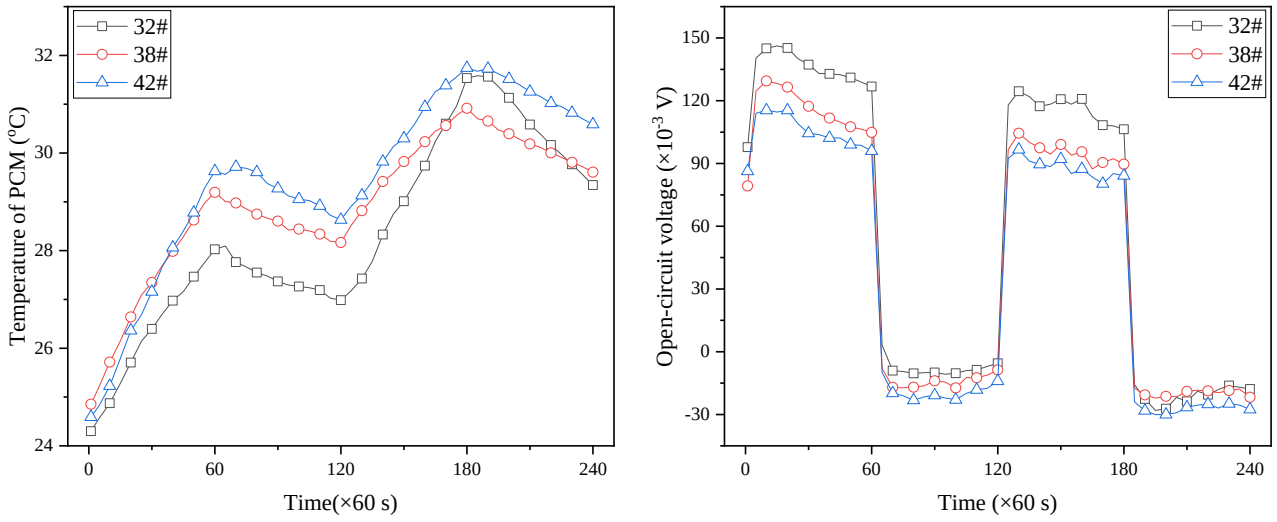

(a) PCM Temperature

(b) Open-circuit voltage

Fig. 4. PCM temperature and open-circuit voltage versus different PCM.

The electrical energy generated by the TEG with different PCM is listed in Table 5. It is seen from the table that an increase in the phase transition temperature of PCM results in a higher average TEG temperature of two surfaces, which also attributes to the increased electrical energy generated by the TEG under three different levels of radiation intensity. Interestingly, more electrical energy is generated by the TEG when the average TEG temperature approaches the phase transition temperature of PCM. Similar conclusions were drawn by Zhu et al. [43] that more electrical energy output could be achieved when the average TEG temperature got closer to the phase transition temperature of PCM. The main reason may be that an increased temperature difference across the TEG leads to a greater power generation potential when the PCM performs a better energy storage and discharge process at the corresponding temperature. However, the output electrical energy may also be affected by the hot-side temperature in addition to the average temperature of two sides of the TEG. It is expected that more electrical energy can be generated by the TEG with a higher hot-side temperature, which can be explained by the temperature dependence of ZT [48], i.e. the higher the operating temperature, the greater the value of ZT.

The electrical energy decreases when the radiation-cooling cycle increases owing to the average PCM temperature being increased gradually, which results in a decreased temperature difference between two surfaces of the TEG. In addition, the increased radiation intensity can lead to a more substantial increase in the electrical energy generation [49]. Therefore, choosing the PCM with appropriate phase transition temperature is critical for improving the electrical energy output as the TEG mean temperature changes with different radiation intensities.

Table 5. Electrical energy output of the TEG under various radiation intensities.

Radiation intensity (W/m^2)	PCM	First cycle		Second cycle		Total electrical energy (J)
		TEG mean temperature (°C)	Electrical energy (J)	TEG mean temperature (°C)	Electrical energy (J)	
615	32#	28.6	2.42	31.2	1.82	4.24
	38#	28.7	1.79	30.7	1.23	3.02
	42#	29.0	1.51	31.5	1.11	2.62
990	32#	31.6	4.99	35.9	3.94	8.93
	38#	31.2	3.60	33.9	3.02	6.62
	42#	30.5	2.77	32.8	2.38	5.15
1330	32#	35.7	10.19	41.7	7.43	17.62
	38#	33.9	7.65	37.4	6.11	13.76
	42#	33.3	6.26	36.1	5.32	11.58

3.1.2. Thickness of the PCM layer

The impact of different thicknesses of the PCM layer in the range of 0.01 m and 0.03 m on the performance of the TEG module coupled with the PCM was investigated. The temperature of the PCM in the middle of the container (T_3) under two radiation intensities of 990 W/m^2 and 1330 W/m^2

is shown in Fig. 5. It indicates that an increase in the PCM layer thickness reduces the temperature variation range. For instance, the temperature at the first radiation stage increases from about 20.7 ºC to 27 ºC, 31.1 ºC and 34.1 ºC for the thicknesses of 0.03 m, 0.02 m and 0.01 m respectively under the radiation intensity of 990 W/m^2, as shown in Fig. 5 (a). This is attributed to the fact that the heat storage capacity of the PCM increases when the thickness of the PCM layer increases. In addition, the temperature of the PCM at the first natural-cooling stage reduces from 27 ºC, 31.1 ºC, 34.1 ºC to 25.4 ºC, 28.1 ºC, 28.7 ºC when the thicknesses of the PCM layer is 0.03 m, 0.02 m and 0.01 m, thereby giving a temperature decrease of 1.6 ºC, 3.0 ºC, 5.4 ºC respectively. At the second radiation and natural-cooling stages, both the maximum and minimum temperature of the PCM increases compared with that at the first cycle. The main reason for this phenomenon is due to the fact that the initial PCM temperature at the second cycle is increased because the heat dissipation at the natural-cooling stage is less than the heat gain at the radiation stage. As more heat is absorbed from the lamp with a larger radiation intensity, the variation range of the PCM temperature is therefore increased, as illustrated by Fig. 5 (b).

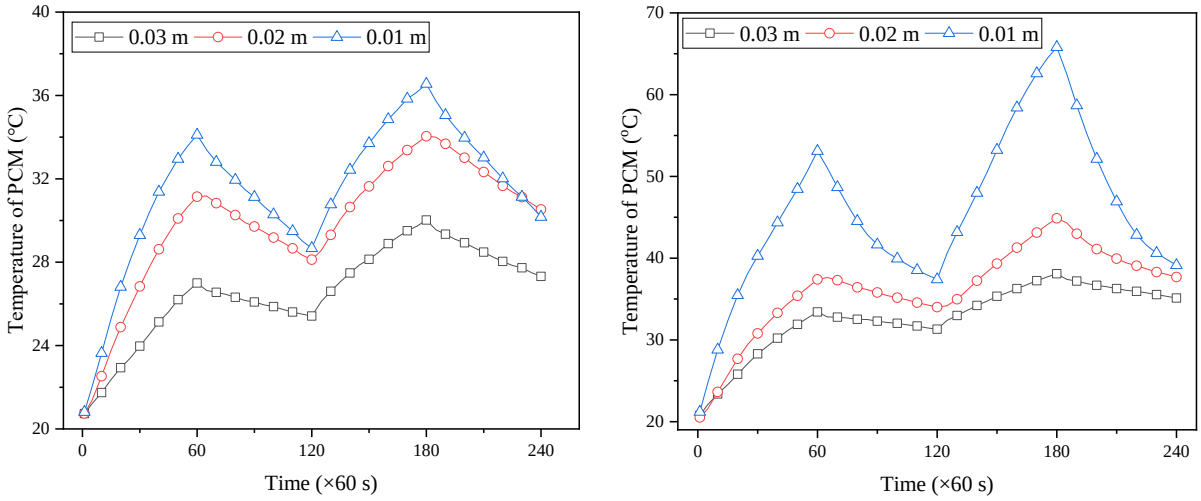

(a) 990W/m^2 (b) 1330 W/m^2

Fig. 5. Temperature of PCM versus different layer thickness.

The open-circuit voltage of the TEG with different PCM layer thickness under radiation intensities

of 990 W/m^2 and 1330 W/m^2 is illustrated in Fig. 6, which shows that the open-circuit voltage increases when the PCM layer thickness increases, and the radiation intensity also has a significant impact on the increase of open-circuit voltage. For instance, the average open-circuit voltage at the heating stage is increased from 0.188 V, 0.174 V and 0.138 V (990 W/m^2) to 0.388 V, 0.343 V and 0.285 V (1330 W/m^2) when the PCM layer thickness is 0.03 m, 0.02 m and 0.01 m respectively. This is because a larger thickness gives the PCM a higher heat capacity, thereby enabling it to absorb a greater amount of thermal energy without an apparent temperature increase, as shown in Fig. 5. Therefore, the smaller the PCM layer thickness, the lower the open-circuit voltage at radiation stage is. A decrease in the PCM layer thickness results in a higher open-circuit voltage at the cooling stage. This can be explained by the fact that a smaller PCM layer thickness results in a higher temperature rise which consequently contributes to a decreased temperature difference between TEG and PCM [50]. As indicated by Fig. 6, the average open-circuit voltage is increased from 0.025 V, 0.039 V and 0.044 V at the first natural-cooling stage to 0.060 V, 0.072 V and 0.101 V at the second natural-cooling stage respectively when the PCM layer thickness is 0.03 m, 0.02 m and 0.01 m (990W/m^2), respectively. A higher PCM temperature however enhances the open-circuit voltage at natural-cooling stage. In addition, an increased dropping rate of the open-circuit voltage is also observed when the PCM layer thickness decreases.

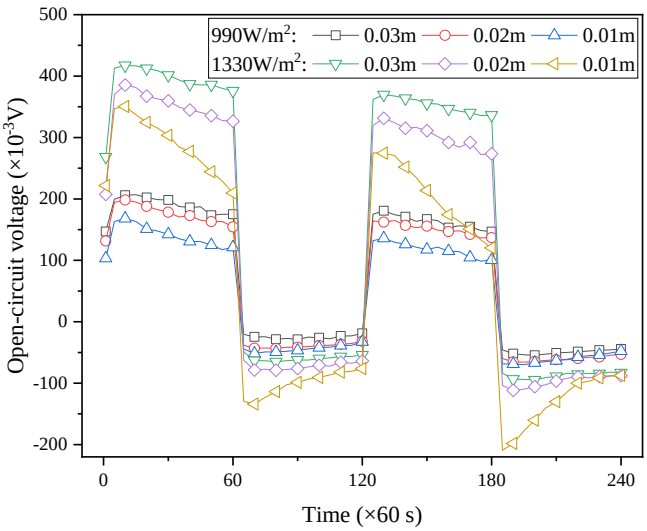

Fig. 6. Open-circuit voltage of TEG versus different PCM layer thickness.

Based on the open-circuit voltage presented in Fig. 6, the total electrical energy generated by the TEG with different PCM layer thickness is listed in Table 6, which shows that both the PCM layer thickness and radiation intensity have a drastic impact on the total electrical energy. The total electrical energy increases from 5.17 J to 7.73 J and 8.61 J when the PCM layer thickness increases from 0.01 m to 0.02 m and 0.03 m under the radiation intensity of 990 W/m^2. Meanwhile, the increase of the radiation intensity from 990 W/m^2 to 1330 W/m^2 has also pushed the total electrical energy to rise by at least 400%. It is expected that the decrease in the PCM layer thickness does not significantly impact the total electrical energy under a lower radiation intensity such as 990 W/m^2. However, the total electrical energy would be apparently affected by the PCM layer thickness under a higher radiation intensity such as 1330 W/m^2. Therefore, it is suggested that the PCM layer thickness should be properly determined according to the radiation intensity or temperature range in the actual working environment.

Table 6 Electrical energy output under different PCM layer thickness.

Thickness of PCM (m)	Electrical energy -990W/m^2 (J)	Electrical energy-1330W/m^2 (J)

0.03	8.61	38.12
0.02	7.73	30.05
0.01	5.17	20.80

3.1.3. Thermal conductivity

Due to the lower thermal conductivity of paraffin ranged between 0.1 W/(m·K) and 0.7 W/(m·K), a series of measures including adding graphite [51, 52], metal nano-particles [53] and fins [54, 55] can be taken to improve the thermophysical properties of PCM. The expanded graphite is mixed with the 38# paraffin to improve its thermal property in this study. The detailed thermophysical parameters of the 38# paraffin improved by adding different mass ratio of expanded graphite are listed in Table 7, which shows that the thermal conductivity increases from the original value of 0.2838 W/(m·K) to 1.1940 W/(m·K) when the mass ratio of expanded graphite increases from zero to 4%. However, DSC results show that the expanded graphite has a negative impact on the phase-change enthalpy of paraffin, which may be caused by the decreased ratio of the PCM in the total expanded graphite-paraffin composite materials.

Table 7 Thermal properties of the 38# paraffin with different mass ratio of graphite.

Mass ratio of expanded graphite	Thermal conductivity (W/(m·K))	Phase change temperature (°C)	Enthalpy (kJ/kg)
0	0.2838	28.3-51.9	116.2
1%	0.3681	27.5-51.0	113.27
2%	0.5955	27.3-50.1	104.77
3%	0.8379	25.5-48.2	101.76
4%	1.1940	26.4-51.1	101.21

As shown in Fig. 7, the PCM temperature and open-circuit voltage with different mass ratio of

expanded graphite is investigated under a PCM layer thickness of 0.03 m and a radiation intensity of 990 W/m^2. As can be seen from Fig. 7 (a), an increase in the mass ratio of expanded graphite leads to a noticeable increase in the PCM temperature. For instance, the PCM temperature is increased by 8.2 ºC, 8.4 ºC, 8.4 ºC and 9.2 ºC when the mass ratio of expanded graphite is 1%, 2%, 3% and 4% respectively, whereas the temperature rise is only 6.7 ºC for the original paraffin without any graphite. This is mainly because the addition of expanded graphite enhances the thermal conductivity and decreases the phase-transition enthalpy of the PCM, thereby allowing more heat to be conducted and stored by the PCM and resulting in a higher temperature rise.

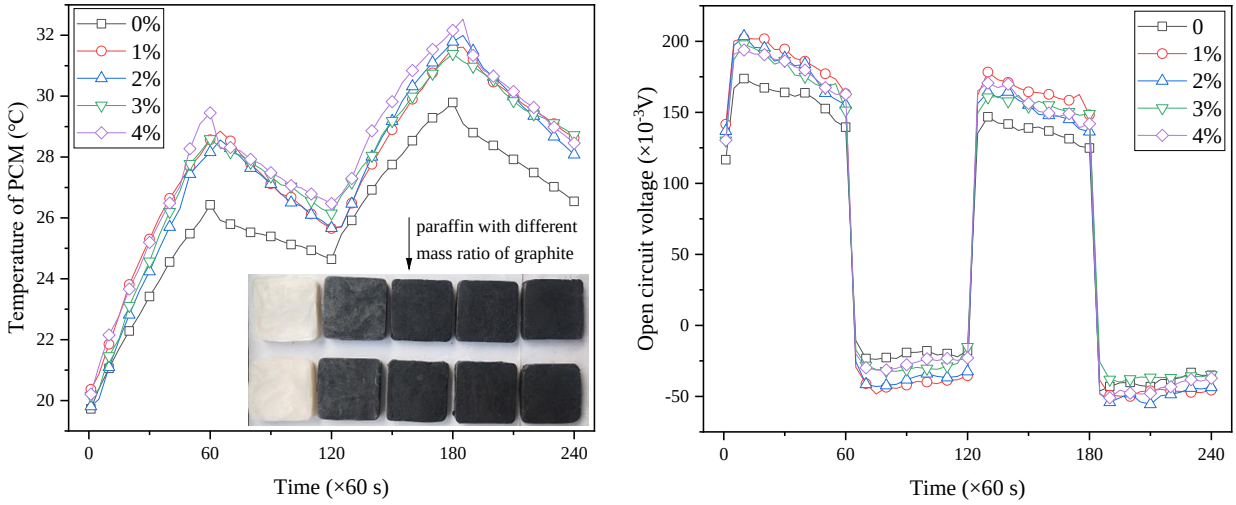

(a) PCM temperature

(b) Open-circuit voltage

Fig. 7. PCM Temperature and open-circuit voltage under different mass ratio of graphite (990W/m^2).

The open-circuit voltage with different mass ratio of expanded graphite is presented in Fig. 7 (b). The results herein reveal the open-circuit voltage increases firstly and then decreases as the mass ratio of expanded graphite increases from 1% to 4%. In details, the achieved maximum open-circuit voltage at the first radiation and natural-cooling stage are 0.175 V and 0.043 V respectively when the mass ratio of expanded graphite is 1%. When the mass ratio of expanded graphite is larger than 1%, it is observed the open-circuit voltage does not strongly depend on the mass ratio of graphite. For instance, the mean open-circuit voltage ranges from 0.166 V to 0.166 V and 0.167 V at the first

radiation stage, and also ranges from 0.043 V to 0.032 V and 0.035 V at the first natural-cooling stage when the mass ratio of graphite increases from 2% to 3%, 4% respectively. The coupled effects of the enhanced thermal conductivity and the decreased phase-transition enthalpy by mixing the PCM with different mass ratio of expanded graphite may contribute to this phenomenon.

The total electrical energy generated by the TEG with different mass ratios of expanded graphite is listed in Table 8, which shows that the electrical energy increases firstly and then decreases slightly when the mass ratio of expanded graphite increases. In details, the achieved maximum electrical energy is 8.62 J when the mass ratio of expanded graphite is 1%. When the mass ratio of expanded graphite is larger than 1%, the total electrical energy decreases slightly, which agrees with the findings in a previous literature [43].

Table 8 Electrical energy of TEG versus different expanded graphite.

Mass ratio of graphite (%)	0	1	2	3	4
Electrical energy (J)	6.01	8.62	7.80	7.55	7.73

3.2. Effects of heat transfer enhancement

3.2.1. Absorption coefficient

The absorptivity of the ceramic surface of TEG was lower than 0.5, which means that more than 50% of total radiation energy is reflected to the surrounding environment. In order to improve the absorption ratio, the TEG surface was coated with carbon and the absorption coefficient was increased from 0.5 to 0.9. The impact of surface coating on PCM temperature and open-circuit voltage under radiation intensity of 990 W/m^2 and 1330 W/m^2 is illustrated in Fig. 8. The increase of the PCM temperature at the radiation stage and temperature drop at natural cooling stage for the coated surface are observed to be larger than those of the original case, and the temperature range also increases when the radiation intensity increases, as shown in Fig. 8 (a). For instance, the PCM temperature is

increased from 18.6 ºC to 30.7 ºC for the coated surface under a radiation intensity of 990 W/m^2, whereas the temperature increases from 18.8 ºC to 27.7 ºC for the untreated surface at the first radiation cycle. At the second natural cooling stage, the PCM temperature decreases from 44.3 ºC to 36.3 ºC for the coated surface under a radiation intensity of 1330 W/m^2, in comparison to the finding that the temperature decreases from 36.2 ºC to 32.1 ºC for the original one. This is mainly attributed to the increased absorption coefficient achieved by the surface treatment which leads to a higher PCM temperature change. In addition, the increase of the PCM temperature at the radiation stage and temperature drop at the natural-cooling stage gradually deceases and increases respectively during the radiation cycles. This impact on the temperature variations may have been caused by the lower heat dissipation and higher heat gains, which consequently leads to a slight increase in the PCM temperature.

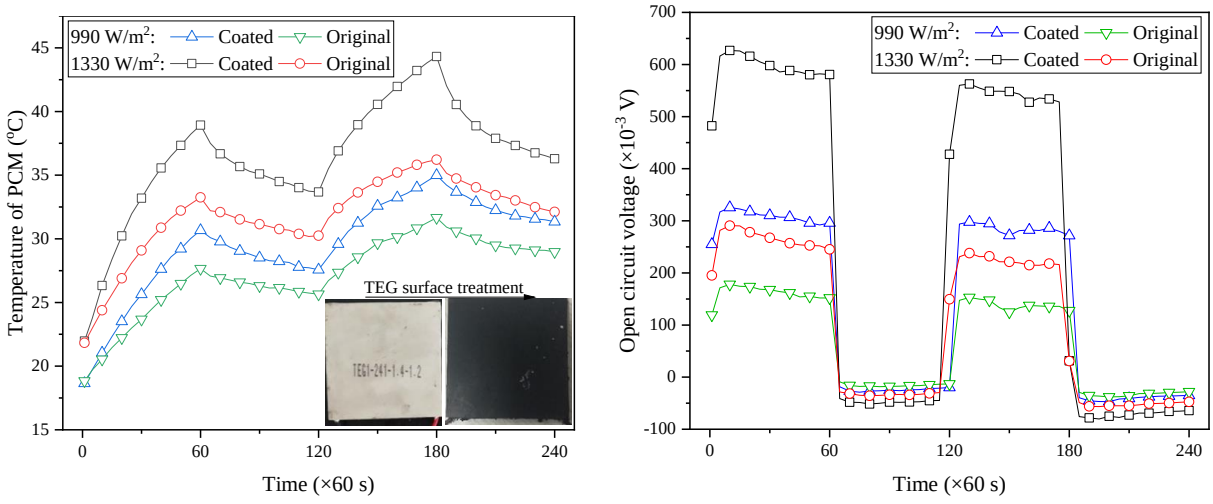

(a) Temperature of PCM (b) Open-circuit voltage

Fig. 8. PCM temperature and open circuit voltage versus different surface treatments.

The open-circuit voltage with/without surface treatment under different radiation intensities is illustrated in Fig. 8 (b), which shows the open-circuit considerably increases when the TEG surface is coated. For instance, the average open-circuit voltage of the coated surface at the radiation and cooling stage is 0.297 V and 0.033 V, compared with 0.153 V and 0.025 V respectively for the original

surface. In addition, the enhancement in the electrical power output achieved by using the coating treatment is more obvious under a higher radiation intensity. The average open-circuit voltage under a radiation intensity of 1330 W/m^2 increases from 0.262 V for the original surface to 0.590 V for the coated surface at the first radiation stage with an increase rate of 126%; whereas the increase rate of the open-circuit voltage under 990 W/m^2 is 89% when the original surface is coated. With a higher radiation intensity, more heat is absorbed by the TEG surface and this increased heat absorption results in a high operating temperature and increased temperature difference between two sides of the TEG, thereby generating more electrical energy. Similarly, the open-circuit voltage of the coated surface at the cooling stage is also observed to be larger than that of the original surface. This is because the coated surface has a higher absorption coefficient, which is consistent with a surface that has a larger emissivity according to the *Kirchhoff's* law [56]. However, the open-circuit voltage at the cooling stage is considerably lower than that at the radiation stage owing to the smaller heat transfer rate at the natural cooling stage.

The electrical energy generated by the TEG with the coated and original surfaces under radiation intensities of 990 W/m^2 and 1330 W/m^2 is listed in Table 9. It suggests that more electrical energy can be generated by the TEG with the coated surface. When the TEG surface is coated, the electrical energy increases from 6.16 J to 23.16 J under a radiation intensity of 990 W/m^2, showing that the electrical energy generated by the TEG with the coated surface is 3.75 times higher than that of the original TEG. A larger increase rate of the electrical energy output is observed when the radiation intensity increases. For instance, the electrical energy increases from 15.91 J to 84.73 J under a radiation intensity of 1330 W/m^2 when the TEG surface is coated, thereby enhancing the electrical energy output by 5.33 times in comparison to the electrical energy generated by the original TEG. The TEG surface should therefore be coated with materials with a high absorption coefficient

especially when the radiation intensity is high.

Table 9 Electrical energy of TEG under different surface treatments.

Surface treatment	Electrical energy - 990W/m^2 (J)	Electrical energy - 1330W/m^2 (J)
Coated	23.16	84.73
Original	6.17	15.91

3.2.2. Convection coefficient

To increase the electrical energy generated by TEG, the convection heat transfer between the TEG surface and the surrounding environment should be weakened at the radiation stage and enhanced as much as possible at the cooling stage. This section presents the investigation of the effect of improved convection heat transfer on the open-circuit voltage and electrical energy using two controlled trials, in which a fan with a wind speed of 3 m/s was used to blow the TEG surface just at the cooling stage for one case and natural cooling was used in the other case. Fig. 9 demonstrates the influence of convection conditions on the PCM temperature and open-circuit voltage under radiation intensities of 990 W/m^2 and 1330 W/m^2. As can be seen from Fig. 9 (a), the forced convection results in an increased convection coefficient which in turn leads to a large decrease in the PCM temperature at the cooling stage. For instance, the PCM temperature reduces by 6.11 ºC for the forced convection case in comparison to 3.64 ºC for the natural cooling case at the first cooling stage. This is mainly because of the higher heat dissipation caused by the forced convection at the cooling stage. It is also observed that the PCM temperature difference between forced convection and natural convection decreases when the radiation intensity increases. The reason lies in the fact that the heat dissipation by forced convection is much lower than heat gain through thermal radiation, which contributes to the decreased effect of forced convection on the PCM temperature when the radiation intensity increases. For instance, the heat gain of the TEG is about 891 W/m^2 when the absorption of the coated

surface is 0.9 with a radiation intensity of 990 W/m^2. However, the mean heat dissipation at the second cooling cycle is 173 W/m^2 and 58 W/m^2 when the wind speed is 3 m/s and 0 m/s, respectively. It is seen that the heat gain at the radiation cycle is much larger than the heat dissipation at the cooling cycle.

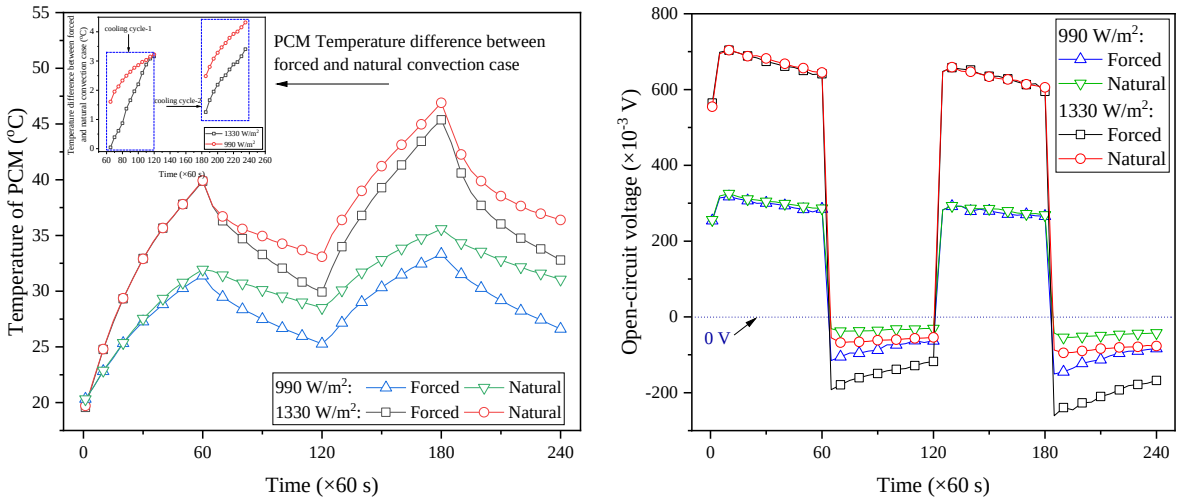

(a) Temperature of PCM (b) Open-circuit voltage

Fig. 9. PCM temperature and open circuit voltage versus different convection conditions.

Fig. 9 (b) illustrates the variation of the open-circuit voltage with different convection conditions. It is clear that the open-circuit voltage with forced convection at the cooling stage is higher than that with natural cooling, which is also consistent with the results of a previous literature [41]. For instance, the average open-circuit voltage of forced convection at the cooling stage is 0.097 V compared with 0.041 V for the natural cooling case. It is considered that the convective heat transfer can be improved by forced convection which leads to a lower surface temperature of the TEG and a greater temperature difference across the TEG. The open-circuit voltage at the second cooling stage is observed to be higher than that at the first cooling stage. This may be caused by the steadily increased PCM temperature which results in a larger temperature difference between the hot and cold side of the TEG.

The total electrical energy generated by the TEG with different convection conditions is listed in Table 10. Although forced convection can improve heat transfer and result in a higher open-circuit

voltage at the cooling stage, the total electrical energy with forced convection is not so obviously increased as originally expected compared with the natural convection case. The reason for that is because the temperature of PCM is not high enough to maintain a high temperature difference across the TEG at the cooling stage. The mean temperature difference at the first and second cooling cycle is 2.4 ºC, 3.3 ºC (forced convection case) and 0.9 ºC, 1.3 ºC (natural convection case), respectively. Meantime, the mean temperature difference at the first and second radiation stage is 8.1 ºC, 7.4 ºC (forced convection case) and 9.0 ºC, 7.1 ºC (natural convection case), respectively. As can also be seen from Fig. 9 (b) that the open-circuit voltage at the cooling stage is much smaller than that at the radiation stage. Although the temperature difference of the forced convection case is larger than that of the natural cooling case, the generated electrical energy at the cooling stage is much lower than that at the radiation stage. For instance, the total electrical energy at the cooling stage and the radiation stage is 5.94 J and 106.48 J respectively for the natural convection case when the radiation intensity is 1330 W/m^2. The electrical energy generated at the cooling stage under forced convection condition only accounts for about 5.28% of the total electrical energy generated by the TEG. Therefore, although the forced convection enhanced the electrical energy output at the cooling stage, the increase is trivial in comparison to the total electrical energy output.

Table 10 Electrical energy output under different convection conditions.

Convection conditions	Electrical energy -990W/m^2 (J)	Electrical energy -1330W/m^2 (J)
Forced	24.12	119.31
Natural	22.72	112.42

4. Conclusions

An experimental investigation on the performance improvement of thermoelectric generators based on phase change materials and heat transfer enhancement is presented in this study. The main findings

are as follows:

(1) The temperature of PCM increases at the radiation stage and decreases slowly at the cooling stage. The lower PCM temperature results in a larger temperature difference between two surfaces of the TEG at the radiation stage, which leads to a higher open-circuit voltage. More electrical energy can be generated when the average TEG temperature approaches the phase transition temperature of PCM. Therefore, a suitable PCM should be selected according to the temperature of hot source to improve the generated electrical energy.

(2) An increase in the PCM layer thickness results in a decreased temperature variation range. The open-circuit voltage increases when the PCM layer thickness increases at the radiation stage and the increase of radiation intensity can contribute to a significant enhancement in the electrical energy output. The PCM layer thickness should be properly determined according to the radiation intensity or temperature range in the actual working environment as the PCM layer thickness has different impacts on the electrical energy output under different radiation intensities.

(3) The thermal conductivity of the applied PCM increases from 0.2838 W/(m·K) to 1.1940 W/(m·K) when the mass ratio of expanded graphite increases from zero to 4%. An increase in the PCM temperature is resulted from the increased mass ratio of expanded graphite. The open-circuit voltage and electrical energy increase firstly and then decrease as the mass ratio of expanded graphite increases from zero to 4%, with the optimal mass ratio of 1%.

(4) The range of the PCM temperature increases when the TEG surface is coated. In addition, the increase in radiation intensity also contributes to the increase in the temperature ranges. The open-circuit considerably increases when the TEG surface is coated, and more electrical energy is generated by the TEG owing to the increased absorption resulted from the surface treatment. The TEG surface is therefore suggested to be coated by materials with high absorption coefficient

to improve the thermoelectric performance.

(5) Forced convection results in an increased convection coefficient and a large decrease in the PCM temperature at the cooling stage. The open-circuit voltage under forced condition at the cooling stage is higher than that under natural cooling. However, the total electrical energy with forced convection is not so obviously increased as expected compared with that under natural convection case.

As a lab-based experimental investigation, this study evaluates how this new PCM-based TEG system concept can utilize the ambient and solar energy, in order to provide technical guidance on how to achieve the optimal system performance. This system concept presents a great potential of supplying electrical energy to devices/facilities in places where there is a poor accessibility to the electricity. However, the practicality and economic viability of such system needs field assessment to identify its suitable application areas.

Acknowledgements

The authors thank the National Natural Science Foundation of China (51978653) and Higher Education Discipline Innovation Project (B14021) for funding this study.

References

[1] Babu C, Ponnambalam P. The role of thermoelectric generators in the hybrid PV/T systems: A review. Energ Convers Manage. 2017;151:368-85.

[2] Karthick K, Suresh S, Hussain MMMD, Ali HM, Kumar CSS. Evaluation of solar thermal system configurations for thermoelectric generator applications: A critical review. Sol Energy. 2019;188:111-42.

[3] Haiping C, Jiguang H, Heng Z, Kai L, Haowen L, Shuangyin L. Experimental investigation of a novel low concentrating photovoltaic/thermal-thermoelectric generator hybrid system. Energy. 2019;166:83-95.

[4] Jaziri N, Boughamoura A, Müller J, Mezghani B, Tounsi F, Ismail M. A comprehensive review of Thermoelectric Generators: Technologies and common applications. Energy Reports. 2019;000:000-.

[5] Pourkiaei SM, Ahmadi MH, Sadeghzadeh M, Moosavi S, Pourfayaz F, Chen LE, et al. Thermoelectric cooler and thermoelectric generator devices: A review of present and potential applications, modeling and materials. Energy. 2019;186.

[6] Huang J, Li W, Guo L, Hu X, Hall JW. Renewable energy and household economy in rural China. Renew Energ. 2020;155:669-76.

[7] Shittu S, Li GQ, Zhao XD, Ma XL. Review of thermoelectric geometry and structure optimization for performance enhancement. Appl Energ. 2020;268.
[8] Champier D. Thermoelectric generators: A review of applications. Energ Convers Manage. 2017;140:167-81.
[9] McCarty R. Thermoelectric Power Generator Design for Maximum Power: It's All About ZT. J Electron Mater. 2013;42(7):1504-8.
[10] Toshima N. Recent progress of organic and hybrid thermoelectric materials. Synthetic Met. 2017;225:3-21.
[11] Gao HB, Huang GH, Li HJ, Qu ZG, Zhang YJ. Development of stove-powered thermoelectric generators: A review. Appl Therm Eng. 2016;96:297-310.
[12] Najjar YSH, Kseibi MM. Heat transfer and performance analysis of thermoelectric stoves. Appl Therm Eng. 2016;102:1045-58.
[13] Orr B, Akbarzadeh A, Mochizuki M, Singh R. A review of car waste heat recovery systems utilising thermoelectric generators and heat pipes. Appl Therm Eng. 2016;101:490-5.
[14] Su HT, Zhou FB, Qi HN, Li JS. Design for thermoelectric power generation using subsurface coal fires. Energy. 2017;140:929-40.
[15] Ding LC, Akbarzadeh A, Tan L. A review of power generation with thermoelectric system and its alternative with solar ponds. Renew Sust Energ Rev. 2018;81:799-812.
[16] Jiang W, Xiao JJ, Yuan DD, Lu HH, Xu SD, Huang Y. Design and experiment of thermoelectric asphalt pavements with power-generation and temperature-reduction functions. Energ Buildings. 2018;169:39-47.
[17] Marandi OF, Ameri M, Adelshahian B. The experimental investigation of a hybrid photovoltaic-thermoelectric power generator solar cavity-receiver. Sol Energy. 2018;161:38-46.
[18] Li GQ, Zhang G, He W, Ji J, Lv S, Chen X, et al. Performance analysis on a solar concentrating thermoelectric generator using the micro-channel heat pipe array. Energ Convers Manage. 2016;112:191-8.
[19] Li GQ, Shittu S, Diallo TMO, Yu M, Zhao XD, Ji J. A review of solar photovoltaic-thermoelectric hybrid system for electricity generation. Energy. 2018;158:41-58.
[20] Li GQ, Shittu S, Ma XL, Zhao XD. Comparative analysis of thermoelectric elements optimum geometry between photovoltaic-thermoelectric and solar thermoelectric. Energy. 2019;171:599-610.
[21] Borset MT, Wilhelmsen O, Kjelstrup S, Burheim OS. Exploring the potential for waste heat recovery during metal casting with thermoelectric generators: On-site experiments and mathematical modeling. Energy. 2017;118:865-75.
[22] Rodrigues CRS, Machado T, Pires AL, Chaves B, Carpinteiro FS, Pereira AM. Recovery of thermal energy released in the composting process and their conversion into electricity utilizing thermoelectric generators. Appl Therm Eng. 2018;138:319-24.
[23] Sun YM, Sheng P, Di CA, Jiao F, Xu W, Qiu D, et al. Organic Thermoelectric Materials and Devices Based on p- and n-Type Poly(metal 1,1,2,2-ethenetetrathiolate)s. Adv Mater. 2012;24(7):932-+.
[24] Culebras M, Gomez CM, Cantarero A. Review on Polymers for Thermoelectric Applications. Materials. 2014;7(9):6701-32.
[25] LeBlanc S, Yee SK, Scullin ML, Dames C, Goodson KE. Material and manufacturing cost considerations for thermoelectrics. Renew Sust Energ Rev. 2014;32:313-27.
[26] Zhang Q, Sun YM, Xu W, Zhu DB. Organic Thermoelectric Materials: Emerging Green Energy Materials Converting Heat to Electricity Directly and Efficiently. Adv Mater. 2014;26(40):6829-51.
[27] Aswal DK, Basu R, Singh A. Key issues in development of thermoelectric power generators: High figure-of-merit materials and their highly conducting interfaces with metallic interconnects. Energ Convers Manage. 2016;114:50-67.
[28] Ming TZ, Yang W, Wu YJ, Xiang YT, Huang XM, Cheng JT, et al. Numerical analysis on the thermal behavior of a segmented thermoelectric generator. Int J Hydrogen Energ. 2017;42(5):3521-35.
[29] Ming TZ, Yang W, Huang XM, Wu YJ, Li XH, Liu J. Analytical and numerical investigation on a new compact thermoelectric generator. Energ Convers Manage. 2017;132:261-71.

[30] Sajid M, Hassan I, Rahman A. An overview of cooling of thermoelectric devices. Renew Sust Energ Rev. 2017;78:15-22.
[31] Zheng XF, Liu CX, Yan YY. Investigations on an oriented cooling design for thermoelectric cogenerations. Journal of Physics: Conference Series. 2012;395:012062.
[32] Seo YM, Ha MY, Park SH, Lee GH, Kim YS, Park YG. A numerical study on the performance of the thermoelectric module with different heat sink shapes. Appl Therm Eng. 2018;128:1082-94.
[33] Zheng XF, Liu CX, Boukhanouf R, Yan YY, Li WZ. Experimental study of a domestic thermoelectric cogeneration system. Appl Therm Eng. 2014;62(1):69-79.
[34] Zheng XF, Yan YY, Simpson K. A potential candidate for the sustainable and reliable domestic energy generation-Thermoelectric cogeneration system. Appl Therm Eng. 2013;53(2):305-11.
[35] Zhang LB, Li RY, Tang B, Wang P. Solar-thermal conversion and thermal energy storage of graphene foam-based composites. Nanoscale. 2016;8(30):14600-7.
[36] Mahmoudinezhad S, Cotfas PA, Cotfas DT, Rezania A, A.Rosendah L. Performance evaluation of a high-temperature thermoelectric generator under different solar concentrations. Energy Procedia. 2018;147:624-30.
[37] Kraemer D, Poudel B, Feng HP, Caylor JC, Yu B, Yan X, et al. High-performance flat-panel solar thermoelectric generators with high thermal concentration. Nat Mater. 2011;10(7):532-8.
[38] Orr B, Akbarzadeh A, Lappas P. An exhaust heat recovery system utilising thermoelectric generators and heat pipes. Appl Therm Eng. 2017;126:1185-90.
[39] Shittu S, Li GQ, Xuan Q, Xiao X, Zhao XD, Ma XL, et al. Transient and non-uniform heat flux effect on solar thermoelectric generator with phase change material. Appl Therm Eng. 2020;173.
[40] Zhang Q, Agbossou A, Feng ZH, Cosnier M. Solar micro-energy harvesting based on thermoelectric and latent heat effects. Part II: Experimental analysis. Sensor Actuat a-Phys. 2010;163(1):284-90.
[41] Agbossou A, Zhang Q, Sebald G, Guyomar D. Solar micro-energy harvesting based on thermoelectric and latent heat effects. Part I: Theoretical analysis. Sensor Actuat a-Phys. 2010;163(1):277-83.
[42] Jaworski M, Bednarczyk M, Czachor M. Experimental investigation of thermoelectric generator (TEG) with PCM module. Appl Therm Eng. 2016;96:527-33.
[43] Zhu W, Tu YB, Deng Y. Multi-parameter optimization design of thermoelectric harvester based on phase change material for space generation. Appl Energ. 2018;228:873-80.
[44] Atouei SA, Ranjbar AA, Rezania A. Experimental investigation of two-stage thermoelectric generator system integrated with phase change materials. Appl Energ. 2017;208:332-43.
[45] Atouei SA, Rezania A, Ranjbar AA, Rosendahl LA. Protection and thermal management of thermoelectric generator system using phase change materials: An experimental investigation. Energy. 2018;156:311-8.
[46] Boriskina S, Tong J, Hsu W-C, Weinstein L, Huang X, Loomis J, et al. Hybrid optical-thermal devices and materials for light manipulation and radiative cooling: SPIE, 2015.
[47] Sullivan TJ. Introduction to Uncertainty Quantification. Switzerland: Springer, 2015.
[48] Hasegawa Y, Otsuka M. Temperature dependence of dimensionless figure of merit of a thermoelectric module estimated by impedance spectroscopy. Aip Adv. 2018;8(7).
[49] Rahbar N, Esfahani JA, Asadi A. An experimental investigation on productivity and performance of a new improved design portable asymmetrical solar still utilizing thermoelectric modules. Energ Convers Manage. 2016;118:55-62.
[50] Darkwa J, Calautit J, Du D, Kokogianakis G. A numerical and experimental analysis of an integrated TEG-PCM power enhancement system for photovoltaic cells. Appl Energ. 2019;248:688-701.
[51] Pincemin S, Olives R, Py X, Christ M. Highly conductive composites made of phase change materials and graphite for thermal storage. Sol Energ Mat Sol C. 2008;92(6):603-13.
[52] Bahraseman HG, Languri EM, East J. Fast charging of thermal energy storage systems enabled by phase change materials mixed with expanded graphite. Int J Heat Mass Tran. 2017;109:1052-8.

[53] Lin SC, Al-Kayiem HH. Evaluation of copper nanoparticles - Paraffin wax compositions for solar thermal energy storage. Sol Energy. 2016;132:267-78.
[54] Gil A, Oro E, Castell A, Cabeza LF. Experimental analysis of the effectiveness of a high temperature thermal storage tank for solar cooling applications. Appl Therm Eng. 2013;54(2):521-7.
[55] Tang XF, Li W, Zhang XX, Shi HF. Fabrication and characterization of microencapsulated phase change material with low supercooling for thermal energy storage. Energy. 2014;68:160-6.
[56] Bergman TL, Lavine AS. Fundamentals of Heat and Mass Transfer: John Wiley & Sons, 2017.